Chinese Chemical Letters 36 (2025) 109569

Contents lists available at ScienceDirect

Chinese Chemical Letters

journal homepage: www.elsevier.com/locate/cclet

Enhanced oxygen reduction reaction on La-Fe bimetal in porous N-doped carbon dodecahedra with CNTs wrapping

Yi Zhou [a,b,1], Yanzhen Liu [b,1], Yani Yan [a,b], Zonglin Yi [b], Yongfeng Li [a,*], Cheng-Meng Chen [b,c,*]

[a] College of Biomedical Engineering, Taiyuan University of Technology, Taiyuan 030024, China
[b] CAS Key Laboratory of Carbon Materials, Institute of Coal Chemistry, Chinese Academy of Sciences, Taiyuan 030001, China
[c] College of Materials Sciences and Opto-Electronic Technology, University of Chinese Academy of Sciences, Beijing 100049, China

ARTICLE INFO

Article history:
Received 11 October 2023
Revised 15 January 2024
Accepted 23 January 2024
Available online 1 February 2024

Keywords:
Electrocatalyst
ORR
Bimetallic nanoparticle
Dendritic CNTs
Zn-air battery

ABSTRACT

The oxygen reduction reaction (ORR) is a crucial process in Zn-air systems, and the catalyst plays a significant role in this reaction. However, reported catalysts often suffer from poor durability and stability during the ORR process. Herein, we synthesized La-Fe bimetallic nanoparticles encapsulated in a N-doped porous carbon dodecahedron (La-Fe/NC) originated from ZIF-8 by a simple direct carbonization. The La-Fe/NC catalyst had a numerous mesopores and dendritic outer layer generated by carbon nanotubes (CNTs), forming a high conductivity network that helped to optimize electron transfer and mass transport in the ORR process. The effect of different doping transition metals and metal ratios on the ORR activity of Zn-air batteries was investigated. In alkaline media, the La-Fe/NC showed the highest ORR catalytic activity, with a half-wave potential ($E_{1/2}$) of 0.879 V (*vs.* RHE, Pt/C 0.845 V). After 5000 cycles, the $E_{1/2}$ of the La-Fe/NC catalyst only decreased by 7 mV, and its performance in stability tests and methanol tolerance tests was superior to Pt/C. When used as the air electrode in a Zn-air battery, the La-Fe/NC catalyst demonstrated an excellent specific capacity of 755 mAh/g and a peak power density of 179.8 mW/cm^2. The results provide important insights for the development of high-performance Zn-air batteries and new directions for the design of ORR catalysts.

With the increasing demand for energy storage in portable electronic devices and electric vehicles, the development of proton exchange membrane fuel cells and metal-air batteries has gained much attention [1–4]. Zn-air batteries have been widely studied, due to their high energy density and low cost. The electrochemical reaction in Zn-air batteries involves oxygen reduction reaction (ORR) at the air electrode and Zn oxidation at the anode [5–7]. ORR plays a critical role in determining the performance of the battery, as it directly affects the efficiency and stability of the air electrode [8,9]. However, the limited electrocatalytic activity of the air electrode and corrosion of the anode restrict the performance and lifespan of the battery. Platinum catalysts (Pt/C) have been extensively used to improve the electrocatalytic activity of the air electrode but are expensive and prone to deactivation [10–12]. Therefore, there is a need for low-cost and efficient electrocatalysts to enhance the overall performance of Zn-air batteries [13–17].

In recent years, extensive research has been conducted on Fe-N-C catalysts [18–20]. However, their durability and stability remain compromised due to the adverse effects of Fenton and demetalation reactions induced by the presence of Fe [21–23]. To address this issue, bimetallic catalysts with unique electronic structures have been proposed. Li *et al.* proposed a synergistic interaction between charge iteration and spin polarization of electrons, which significantly improves the ORR catalytic performance [24]. Under the influence of Ni-Fe bimetallic pairs, the positioning of Fe atoms on the catalyst surface is enhanced, creating stable active sites. This enhances the uptake and catalytic potential of O_2 molecules, thereby promoting the ORR reaction. Zhao *et al.* found that FeMn also exhibits bimetallic synergistic effects. FeMn-N-C synthesized by the encapsulation-ligand exchange strategy, demonstrates excellent electrochemical performance under alkaline and acidic conditions [25]. Because of the low conductivity of bimetallic catalysts, using ZIF-8 as a catalyst support can improve their conductivities [26,27]. Additionally, ZIF-8, rich in nitrogen, can form active sites on the catalyst surface, enabling the adsorption and activation of reactant molecules and facilitating electrocatalytic reactions [28–30]. The previous works have shown that the introduction of metals can promote the growth of carbon nanotubes (CNTs) on ZIF-8,

* Corresponding authors.
E-mail addresses: liyongfeng@tyut.edu.cn (Y. Li), ccm@sxicc.ac.cn (C.-M. Chen).
[1] These authors contributed equally to this work.

https://doi.org/10.1016/j.cclet.2024.109569
1001-8417/

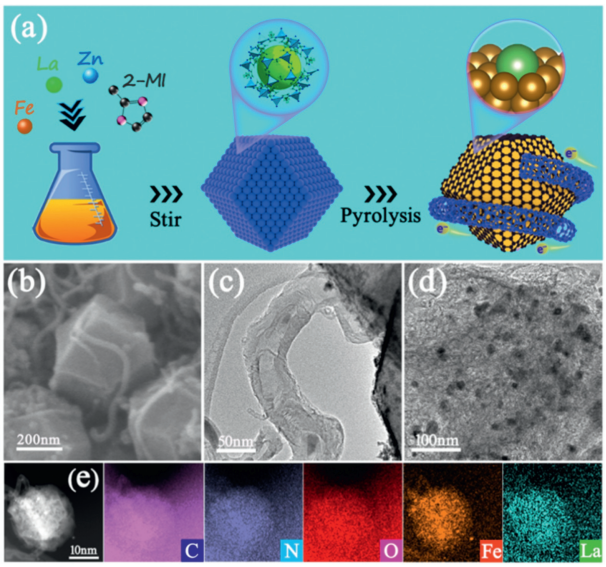

Fig. 1. (a) The synthesis procedure of the La-Fe/NC. (b) SEM image of La-Fe/NC. (c) TEM image of CNT. (d) TEM image of La-Fe/NC. (e) HAADF-STEM image with its respective elemental mapping images.

leading to the formation of a conductive network [31–33]. La element has high chemical activity, can form various oxidation states, and has strong oxidizing properties, which makes La have important applications in fields such as fuel cells and catalysts [34].

Herein, a nitrogen-doped porous carbon dodecahedron decorated with CNTs(NC)and La-Fe bimetallic nanoparticle composite (La-Fe/NC) was synthesized by a simple approach. Because of the presence of Fe-N_4 active sites, the catalyst exhibits excellent ORR activity and durability. Meanwhile, the abundant pores and high specific surface area in the carbon matrix improve the utilization efficiency of active sites [35]. The catalyst exhibited a half-wave potential of 0.879 V *vs*. RHE, indicating its high catalytic efficiency. Moreover, the La-Fe/NC sample was used as an air electrode catalyst in a Zn-air battery, achieving a remarkable specific capacity of 755 mAh/g and a peak power density of 179.8 mW/cm^2, while maintaining stable cycling performance after 5000 cycles of charge-discharge. These results demonstrate the potential of the La-Fe/NC as a superior ORR catalyst in practical Zn-air batteries. Furthermore, the significant contribution of the N-doping strategy and tailored structure design to the exceptional performance of the composite catalyst is highlighted.

The La-Fe/NC catalyst was prepared by using 2-methylimidazole as a carbon source to encapsulate metal nanoparticles and form precursors, followed by carbonization at 900 °C under an Ar atmosphere (Fig. 1a). For comparison, the various catalysts, such as NC, Fe/NC, La/NC, 0.5La-Fe/NC, La-Fe/NC, and 1.5La-Fe/NC were also synthesized under different conditions (see Supporting information). ZIF-8 is a type of metal-organic framework (MOF) with a series of orthogonal pores formed by metal ions and organic ligands. The size and shape of these pores can be precisely controlled, providing a highly tunable pore size and porosity. In addition, the evaporation of Zn in the precursor mixture at around 900 °C leads to the formation of numerous micro- and mesopores in ZIF-8 [30,36,37]. During pyrolysis, the specific proportion of Fe nanoparticles and 2-methylimidazole induces *in situ* growth of CNTs with a diameter of about 30 nm, and TEM images of La-Fe/NC with numerous CNTs coated on the surface of carbon dodecahedron (Fig. 1b and Fig. S1 in Supporting information) [38]. After CNT growth, not only did it increase the surface area and active sites of the catalyst, but it also formed a highly conductive network [39]. Additionally, the growth of carbon nanotubes in the ZIF-8 encapsulated catalyst has a positive impact on its catalytic performance, which can adjust the pore structure and enhance conductivity, as well as dispersing the carbon dodecahedron to avoid adhesion [40]. The TEM images of catalysts with different metal dopings are shown in Fig. S2 (Supporting information). In Figs. 1c and d, it can be seen that metal nanoparticles with a diameter of about 8 nm are uniformly dispersed in CNTs and carbon dodecahedra. The elemental distribution of La-Fe/NC was assessed using EDS technology. Fig. 1e shows the homogeneous distribution of C, N, O, La, and Fe ions in the sample.

The XRD patterns (Fig. S4a in Supporting information) show peaks at around 25.3°, 44.4°, and 53.1° for the 0.5La-Fe/NC and La-Fe/NC samples, corresponding to the (002), (101), and (102) planes of graphite carbon which is mainly attributed to CNTs (Fig. S3a in Supporting information) [41,42]. In addition, diffraction peaks associated with Fe element were observed at (110) and (211) planes, and a weak diffraction peak corresponding to the (331) plane of La element is observed, which are consistent with the results in HRTEM (Figs. S3b and c in Supporting information) [43]. Raman spectroscopy was employed to assess the level of graphitization in carbon materials used as catalysts [44]. Among the samples, including NC, a/NC, Fe/NC, 0.5La-Fe/NC, and 1.5La-Fe/NC, the La-Fe/NC catalyst exhibited a lower I_D/I_G value of 0.95 compared to others (Fig. S4b in Supporting information). This suggested a higher degree of graphitization in the La-Fe/NC catalyst. The N_2 adsorption-desorption isotherms show that 0.5La-Fe/NC, La-Fe/NC, and 1.5 La-Fe/NC all exhibit IV-type adsorption isotherms, belonging to the H4-type hysteresis loop (Fig. S5 in Supporting information) [45]. This indicates that the catalysts have a mixed pore size distribution between micropores and mesopores, as well as a highly interconnected pore structure that facilitates the diffusion of O_2 molecules in the pores. The specific surface area of La-Fe/NC is 513 m^2/g, slightly higher than that of 0.5 La-Fe/NC and 1.5 La-Fe/NC (Table S1 in Supporting information).

XPS analysis is used to analyze the different types and contents of elements in these catalysts. Characteristic XPS peaks were observed for the obtained samples (Fig. S6a and Table S2 in Supporting information). The N 1s spectrum of La-Fe/NC can be decomposed into five peaks located at 404.5, 401.1, 400.1, 398.9 and 397.8 eV representing oxidized N, graphitic N, pyrrolic N, metal-N (M-N) and pyridinic N, respectively (Figs. 2a and b, Table S3 and Fig. S7a in Supporting information) [46,47]. The addition of metal N in bimetallic ORR catalysts improves the selectivity of the catalyst and can also form active sites on the catalyst surface, promoting the adsorption and dissociation of O_2 molecules, and enhancing the ORR reaction rate. The NC does not contain metal nanoparticles, so no metal N peak appears in the N 1s XPS analysis. This means that there is no bond between metal N and N atoms, leading to a decrease in the number of active sites on the catalyst surface and the ORR reaction rate. The addition of metal N to the ORR catalyst improves the selectivity of the catalyst, and Fe-N_4 active sites are formed on the catalyst surface, as Fe-N_4 sites are the active species of La-Fe/NC catalyst, thereby increasing the ORR reaction rate [48,49]. The C 1s spectrum of the La-Fe/NC sample was divided into four sub-peaks corresponding to C–O, C–N, C=N and C–C, located at 289, 286.5, 285.2, and 284.5 eV, respectively (Fig. 2c and Fig. S6b in Supporting information). The presence of C–O, C–N, C=N, and C–C chemical bonds can form bonding interactions between metal atoms and O/N atoms, thereby forming active sites on the surface of bimetallic catalysts and promoting the adsorption and electron transfer of O_2 molecules in the ORR reaction [46,50]. The formation of C=N and C=C chemical bonds can increase the number of reaction intermediates and promote the progress of the reaction [51]. The O 1s spectrum of La-Fe/NC shows three sub-peaks, with the O1, O2, and O3 peaks located at 530.9,

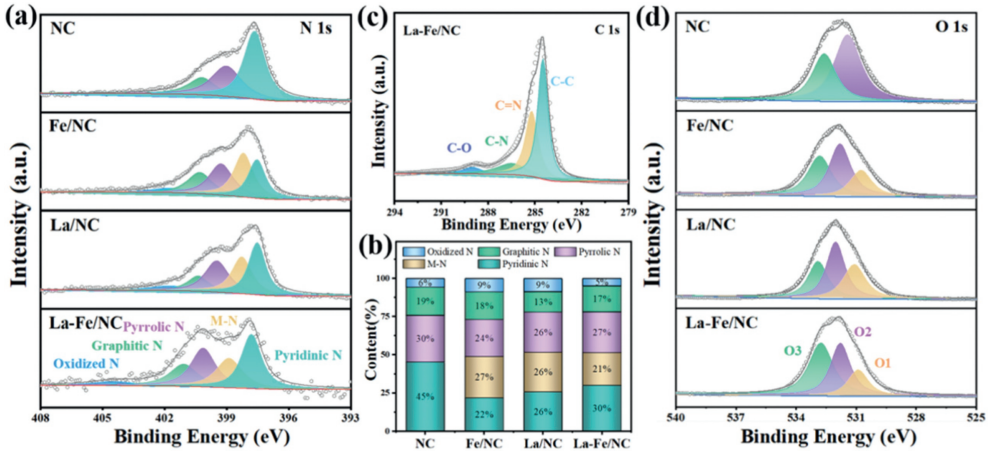

Fig. 2. (a) XPS N 1s spectra of the different samples. (b) The composition of different nitrogen species in the samples. (c) XPS C 1s spectrum of La-Fe/NC. (d) O 1s spectra of NC, Fe/NC, La/NC, and La-Fe/NC.

531.8, and 532.8 eV, respectively (Fig. 2d and Fig. S7b in Supporting information) [52]. The O3 peak corresponds to the metal-oxygen bond, which is a strong chemical bond that can stably adsorb on the metal surface, providing more oxide sites and improving the ORR reaction. The O2 peak corresponds to the incomplete coordination of O_2 on the surface of small-sized materials, indicating that the O_2 coordination on the material surface is incomplete, which can provide more reaction sites and increase the catalytic activity of the ORR reaction. The O1 peak corresponds to chemisorbed O_2 on the surface, which is a weak adsorption state of O_2 and loses electrons in the ORR reaction, thereby participating in the charge transfer of the ORR reaction and increasing the electron transfer rate of the ORR [53,54]. In Fig. S8a (Supporting information), the Fe 3d spectrum of La-Fe/NC was decomposed into four peaks located at 723.5, 720.5, 711.4, and 709.2 eV. Meanwhile, the two peaks at 718.4 and 707.2 eV are contributed by Fe^0. Fe^{3+} and Fe^{2+} are commonly used as active centers for catalyzing the ORR [55]. Fe^{3+} has five paired 3d electrons, and Fe^{3+} gains an electron and can be reduced to Fe^{2+} by the oxidant in the reduction process. Fe^{2+} has four paired 3d electrons and can be oxidized to Fe^{3+} by the action of an oxidant, this dynamic equilibrium contributes to improving the efficiency and catalytic activity of the ORR. Fe^{2+} acts as an electron transfer catalyst, facilitating the reduction of O_2 molecules and providing a reaction pathway for electron transfer [56]. In Fig. S8b (Supporting information), the La 3d spectrum was decomposed into four peaks located at 854.9, 851.5, 838.2, and 834.1 eV. La^{3+} can act as one of the catalytic centers in the ORR reaction by adsorbing electrons from O_2 molecules to facilitate the ORR reaction [57,58]. The interaction between the 3D electronic energy levels of La atoms and O_2 molecules can regulate the electronic structure and redox performance of catalyst materials, making it easier for La nanoparticles to participate in the reaction [59]. The nitrogen functional groups on the NC surface provide high-density active sites, excellent electron transfer and surface polarity adjustment capabilities [46]. Therefore, the ORR activity is significantly improved under the interaction between La-Fe metal nanoparticles and NC.

The ORR electrocatalytic performance of the La-Fe/NC catalyst was investigated in a saturated oxygen-containing 0.1 mol/L KOH electrolyte. The La-Fe/NC exhibits excellent ORR half-wave potential ($E_{1/2}$) of 0.879 V (Fig. 3a), outperforming that of NC (0.69 V), Fe/NC (0.808 V), La/NC (0.733 V), 0.5La-Fe/NC (0.87 V), 1.5La-Fe/NC (0.787 V), and 20 wt% Pt/C (0.845 V), which surpasses many previously reported bimetallic catalysts (Table S4 in Supporting information). In the La-Fe catalyst, the optimal performance was achieved when Fe and La are in a 1:1 molar ratio (Fig. S9a in Supporting information, named as La-Fe/NC), as this may create the most balanced electron interaction on the catalyst surface and establish an optimal electron environment. The onset potential of the La-Fe/NC catalyst ($E_{onset} = 1.12$ V) is higher than that of Pt/C ($E_{onset} = 1.08$ V). At 0.80 V *vs.* RHE, the La-Fe/NC achieves the kinetic current density (J_K) of 4 mA/cm^2, higher than Pt/C (3.5 mA/cm^2). The enhanced electrocatalytic activity of La-Fe/NC can be attributed to the balanced electronic interaction between Fe and La, which promotes the formation of favorable adsorption sites and electron environments on the bimetallic catalyst surface, maximizing the ORR activity. Moreover, the Tafel slope of La-Fe/NC was found to be 77.29 mV/dec (Fig. 3b and Fig. S9b in Supporting information), which is significantly lower than that of the NC (175.78 mV/dec), Fe/NC (137.03 mV/dec), La/NC (244.13 mV/dec), and Pt/C (90.33 mV/dec). The excellent electron transfer capability combined with optimized electronic structure gives La-Fe/NC a competitive advantage in terms of activity and efficiency. The H_2O_2 generation of La-Fe/NC averages about 1.72% (Fig. 3c and Fig. S9c in Supporting information), significantly lower than that of the NC (10.8%), Fe/NC (4.6%), La/NC (5.4%), and Pt/C (2.07%), indicating that the enhanced activity and selectivity. The test result of ORR electron transfer number is about 3.97, which is consistent with the slope calculated by the K-L equation, indicating a direct 4e transfer process (Fig. S9d in Supporting information). A reasonable La-Fe molar ratio can promote the occurrence of combined effects. As shown in Fig. S1f, a large amount of La can hinder the production of CNTs, inhibit the dispersion of carbon dodecahedra, and lead to partial fusion, resulting in a decrease in performance. Furthermore, the La-Fe/NC catalyst also demonstrates excellent a long-term stability (Fig. 3d). The $E_{1/2}$ of the La-Fe/NC only experiences a slight 7 mV attenuation after 5000 potential cycles, while the Pt/C exhibits a potential decay of 24 mV under the same conditions. This stability is essential for maintaining consistent long-term ORR performance. After a current response measurement of 20,000 s (Fig. 3e), the normalized current retention rate of La-Fe/NC is 90.1%, surpassing commercial Pt/C (80.2%). Additionally, the methanol tolerance test can assess the catalyst's blocking effect on methanol, preventing unnecessary oxidation reactions during the ORR process. Unlike Pt/C, the current density of the La-Fe/NC catalyst exhibits minimal fluctuations upon methanol injection, indicating the excellent selectivity and resistance to interference of La-Fe/NC (Fig. 3f). Therefore, the La-Fe/NC catalyst exhibits outstanding performance in the ORR, surpassing the commercial Pt/C and other control samples. It can be attributed to the combined effect between

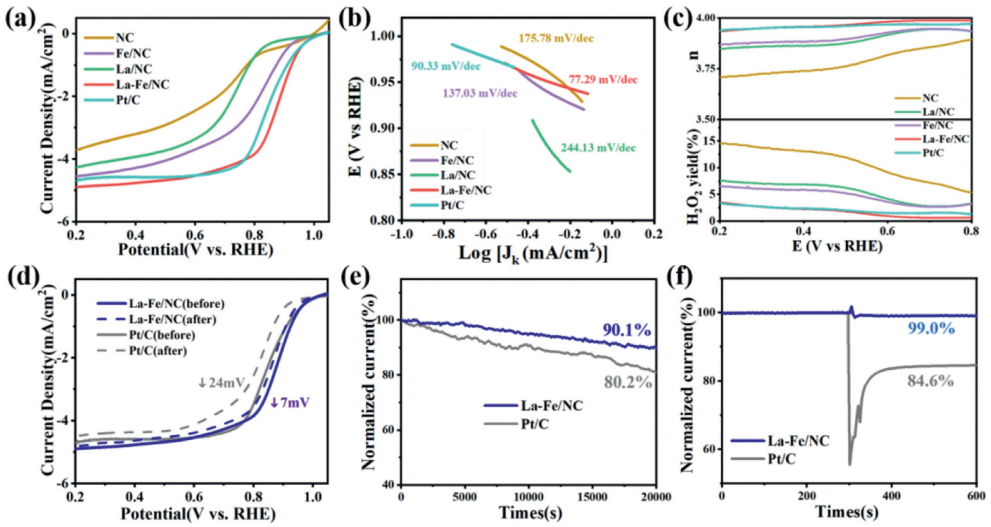

Fig. 3. The catalysts' ORR performance was evaluated in a 0.1 mol/L KOH electrolyte under O_2-saturated conditions. (a) LSV curves, (b) Tafel slopes, (c) electron transfer numbers, and H_2O_2 yields of the NC, Fe/NC, La/NC, La-Fe/NC and 20 wt% Pt/C samples. (d) LSV curves of La-Fe/NC and 20 wt% Pt/C before and after 5000 cycles. (e, f) Curves of the catalyst durability and methanol tolerance.

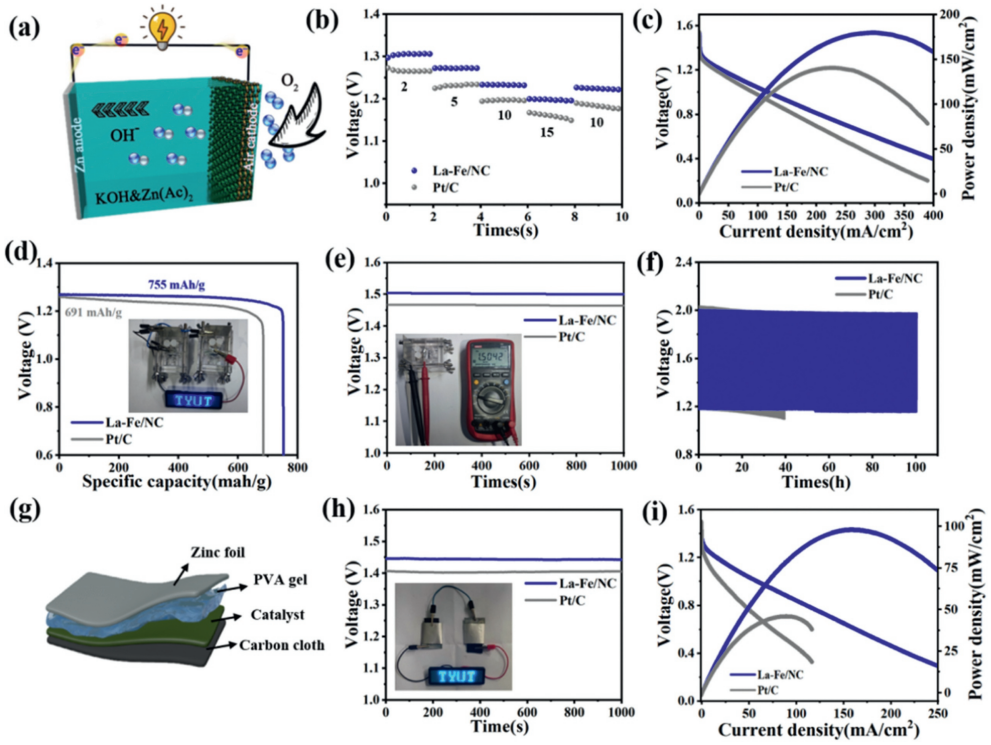

Fig. 4. (a) Schematic diagram of the working principle of a Zn-air battery. (b) 2-h discharge curves of Zn-air batteries assembled with La-Fe/NC and Pt/C catalysts at different current densities. (c) The polarization curves and power density curves. (d) The discharge characteristic curves of a Zn-air battery using La-Fe/NC and Pt/C as catalysts at a discharge current density of 10 mA/cm^2. Inset: Two LEDs illuminated by the ZAB powered by La-Fe/NC. (e) OCV curves of a Zn-air battery utilizing La-Fe/NC and Pt/C as catalysts. Furthermore, an inset optical image showcases the ZAB incorporating La-Fe/NC, exhibiting an OCV of 1.5042 V. (f) Cycling performance of a Zn-air battery based on La-Fe/NC and Pt/C at a current density of 5 mA/cm^2 (6.0 mol/L KOH with 0.2 mol/L Zn acetate used as the electrolyte). (g) A schematic diagram depicting the structure of an all-solid-state Zn-air battery. (h) OCV curves of the all-solid-state Zn-air batteries. Inset: LEDs driven by two all-solid-state Zn-air batteries based on La-Fe/NC. (i) The discharge polarization curves and the corresponding power density plots of the all-solid-state Zn-air batteries.

Fe and La, the source of dense active sites, improved structural stability, excellent electron transfer facilitated by CNTs, and ultimately enhanced selectivity and resistance to interfering species.

The La-Fe/NC catalyst was used to construct a rechargeable Zn-air Battery (ZAB) with an air cathode (Fig. 4a). A comparative study was conducted with a commercially available Pt/C-based ZAB under the same conditions using electrochemical tests. Constant current discharge measurements showed that the La-Fe/NC-based ZAB exhibites a stable voltage plateau of 2 h at 1.31, 1.27, 1.24, and 1.21 V for discharge current densities of 2, 5, 10 and 15 mA/cm^2, respectively (Fig. 4b). These results indicate that the La-Fe/NC catalyst as an air cathode shows, the rapid reaction rate of ORR. The La-Fe/NC-based ZAB exhibited an excellent peak power density of 179.8 mW/cm^2 (Fig. 4c), higher than the Pt/C-based ZAB with

140.5 mW/cm^2. Furthermore, the La-Fe/NC-based ZAB displayed an outstanding specific capacity of 755 mAh/g at 10 mA/cm^2 compared to the Pt/C-based ZAB with only 691 mAh/g (Fig. 4d). Moreover, the two ZABs combined as a power source were able to power an LED light bulb. The bimetallic catalyst may have more active centers compared to the commercial Pt/C, thereby improving the catalytic activity.

Furthermore, the open-circuit voltage (OCV) of the La-Fe/NC-based ZAB is 1.504 V (Fig. 4e), while the Pt/C-based ZAB has an OCV of only 1.460 V. As shown in Fig. 4f, the cycling performance of both ZABs was tested through charge and discharge cycles of 20 min. The La-Fe/NC-based ZAB maintaines stability for 100 h at 5 mA/cm^2 with no significant decay. In contrast, the Pt/C-based ZAB exhibited a gradual decrease in discharge voltage platform after cycling for 30 h. We also assembled a solid-state Zn-air battery in an alkaline electrolyte. The battery consisted of Zn foil, PVA gel electrolyte and the catalyst attached to a carbon cloth (Fig. 4g). The La-Fe/NC based solid-state ZAB had a OCV of 1.445 V (Fig. 4h) and a peak power density of 97.9 mW/cm^2 (Fig. 4i). Notably, these performances surpassed those of the Pt/C-based solid-state ZAB with an OCV of 1.404 V and a peak power density of 45.9 mW/cm^2. By connecting two La-Fe/NC-based solid-state Zn-air batteries (ZABs) in series, a robust and sustainable power supply was achieved for an LED light module. This result highlights the significant potential of this flexible device for various practical applications.

In summary, A nitrogen doped porous carbon dodecahedral decorated with CNTs and La-Fe bimetallic nanoparticle composite (La-Fe/NC) has been prepared by a one-step carbonization method. The growth of CNTs better dispersed the carbon dodecahedra and significantly improved the performance of the catalyst by improving electron transfer efficiency. The interaction between La and Fe, controlled by ZIF-8, results in a highly active catalyst surface of La-Fe/NC. The Fe-N_4 active site improves the efficiency and stability of the catalyst. The synthesized La-Fe/NC catalyst exhibits excellent activity and low H_2O_2 yield in 0.1 mol/L KOH, n close to 4, E_{onset} of 1.12 V, and $E_{1/2}$ of 0.879 V, and its excellent long-term durability and methanol tolerance are superior to Pt/C. Additionally, with an OVC of 1.504 V, peak power density of 179.8 mW/cm^2, and specific capacity of 755 mAh/g, the La-Fe/NC-based Zn-air battery demonstrates excellent performance. Therefore, the feasibility design of La-Fe/NC provides promising prospects for replacing platinum-based catalysts, making significant contributions to further developments in the field of sustainable energy.

Declaration of competing interest

The authors declare that they have no known competing financial interests or personal relationships that could have appeared to influence the work reported in this paper.

Acknowledgments

This work was supported by the National Natural Science Foundation of China (No. 22278291), the Natural Science Foundation of Shanxi Province (Nos. 202203021211145 and 202303021221257), the National Key Research and Development (R&D) Program of China (No. 2020YFB1505803) and the Key Research and Development (R&D) Projects of Shanxi Province (No. 202102070301018).

Supplementary materials

Supplementary material associated with this article can be found, in the online version, at doi:10.1016/j.cclet.2024.109569.

References

[1] H. Wang, K. Wang, Y. Zuo, et al., Adv. Funct. Mater. 33 (2023) 2210127.
[2] M. Li, X. Bi, R. Wang, et al., Matter 2 (2020) 32–49.
[3] K. Chen, X. Wang, C. Zhang, et al., Mater. Today Energy. 30 (2022) 101150.
[4] Y. Chen, E. Chen, Z. Wang, et al., Nano Energy 104 (2022) 107929.
[5] D. Deng, J. Qian, X. Liu, et al., Adv. Funct. Mater. 32 (2022) 2203471.
[6] J. Wang, C. Zhao, J. Liu, et al., Particuology 77 (2023) 146–152.
[7] J.N. Liu, C.X. Zhao, D. Ren, et al., Adv. Mater. 34 (2022) 2109407.
[8] C. Tang, B. Wang, H. Wang, et al., Adv. Mater. 29 (2017) 1703185.
[9] X. Chen, M.X. Li, J.L. Yan, et al., New Carbon Mater. 39 (2024) 78–99.
[10] Z. Yan, L. Gao, C. Dai, et al., Int. J. Hydrogen Energy 43 (2018) 3705–3715.
[11] P. Weber, M. Werheid, M. Janssen, et al., ECS Trans. 86 (2018) 433.
[12] X.X. Xu, N.C. Zhang, J.Y. Wang, New Carbon Mater. 38 (2023) 154–160.
[13] X. Yang, X. Zheng, H. Li, et al., Adv. Funct. Mater. 32 (2022) 2200397.
[14] B. Prakoso, M.A.A. Mahbub, M. Yilmaz, ChemNanoMat 7 (2021) 354–367.
[15] D.C. Nguyen, D.T. Tran, T.L.L. Doan, et al., Adv. Energy Mater. 10 (2020) 1903289.
[16] T. Li, Z. He, X. Liu, et al., Surf. Interf. 33 (2022) 102270.
[17] C.X. Zhao, J.N. Liu, N. Yao, et al., Renewables 1 (2023) 73–80.
[18] Y. He, S. Liu, C. Priest, et al., Chem. Soc. Rev. 49 (2020) 3484–3524.
[19] A. Friedman, L. Landau, S. Gonen, et al., ACS Catal. 8 (2018) 5024–5031.
[20] K. Sheng, J. Li, G. Li, et al., Appl. Surf. Sci. 601 (2022) 154221.
[21] P.G. Santori, F.D. Speck, J. Li, et al., J. Electrochem. Soc. 166 (2019) F3311–F3320.
[22] X. Xie, C. He, B. Li, et al., Nat. Catal. 3 (2020) 1–11.
[23] F. Qin, J. Wang, Y. Liu, A.C.S. Sustain, Chem. Eng. 10 (2022) 7031–7040.
[24] H. Li, J. Wang, R. Qi, et al., Appl. Catal. B: Environ. 285 (2021) 119778.
[25] S. Zhao, Z. Ma, Z. Wan, et al., J. Colloid Interface Sci. 642 (2023) 800–809.
[26] H. Yang, A. Xie, Y. Tang, et al., Chem. Eur J. 28 (2022) e202103275.
[27] Y. Wang, J. Zhou, Y. He, et al., J. Solid State Chem. 302 (2021) 122415.
[28] W. Xue, Q. Zhou, F. Li, et al., J Power Sources 423 (2019) 9–17.
[29] M. Thomas, R. Illathvalappil, S. Kurungot, et al., ACS Appl. Mater. Interfaces 8 (2016) 29373–29382.
[30] Q. Wang, Y. Dai, X. Ruan, et al., J. Membr. Sci. 630 (2021) 119323.
[31] X.M. Qu, S.H. Yin, Y.N. Yan, et al., Chem. Eng. J. 461 (2023) 142054.
[32] I. Dönges, M.I. Büschges, C. Njel, et al., Dalton Trans. 51 (2022) 13725–13733.
[33] R. Kumar, M. Mooste, Z. Ahmed, et al., Ind. Chem. Mater. 1 (2023) 526–541.
[34] Y. Jing, Z. Cai, C. Liu, et al., ACS Catal. 10 (2020) 1010–1023.
[35] U. Martinez, S. Komini Babu, E.F. Holby, et al., Adv. Mater. 31 (2019) 1806545.
[36] R. Yun, B. Zhang, C. Qiu, et al., Inorg. Chem. 60 (2021) 9757–9761.
[37] H.M. Zhang, G.Z. Wang, R.R. Liu, et al., Carbon 106 (2016) 74–83.
[38] W. Li, W. Ding, Y. Nie, et al., ACS Appl. Mater. Interfaces 11 (2019) 22290–22296.
[39] R. Zhu, Y. Zhu, H. Xian, et al., Appl. Catal. B: Environ. 270 (2020) 118891.
[40] L.E. Mphuthi, E. Erasmus, E.H. Langner, ACS Omega 6 (2021) 31632–31645.
[41] T. Huang, H. Fang, S. Mao, et al., Carbon 126 (2018) 566–573.
[42] Y. Zhou, X. Cheng, B. Tynan, et al., Carbon 184 (2021) 504–513.
[43] X. Yu, G. Li, S. Tao, et al., ChemCatChem 15 (2023) e202201612.
[44] M.X. Song, L.J. Xie, J.Y. Cheng, et al., J. Energy Chem. 66 (2022) 448–458.
[45] L. Liu, Q. Kuang, S. Xu, et al., J. Mol. Liq. 380 (2023) 121780.
[46] Z. Zhang, H. Zhang, Y. Hou, et al., J. Mater. Chem. A 10 (2022) 13013–13020.
[47] X. Xie, L. Peng, H. Yang, et al., Adv. Mater. 33 (2021) 2101038.
[48] Y. Zhu, W. Zhou, J. Yu, et al., Chem. Mater. 28 (2016) 1691–1697.
[49] K. Liu, J. Fu, Y. Lin, et al., Nat. Commun. 13 (2022) 2075.
[50] A. Sivanantham, P. Ganesan, S. Shanmugam, Appl. Catal. B: Environ. 237 (2018) 1148–1159.
[51] B. Ge, F. Wei, Q. Wan, et al., J. Phys. Chem. C 126 (2022) 10053–10060.
[52] L. Pei, Y. Song, M. Song, et al., Electrochim. Acta 368 (2021) 137651.
[53] V. Kumar, V. Kumar, S. Som, et al., J. Alloys Compd. 594 (2014) 32–38.
[54] J.Y. Park, Y.S. Jung, J. Cho, et al., Appl. Surf. Sci. 252 (2006) 5877–5891.
[55] Z.Y. Mei, S. Cai, G. Zhao, et al., Energy Storage Mater. 50 (2022) 12–20.
[56] Q.D. Ruan, R. Feng, J.J. Feng, et al., Small 19 (2023) 2300136.
[57] X. Sun, P. Guo, Y. Sun, et al., Materials 14 (2021) 2224.
[58] B. He, C. Li, Z. Xiao, et al., React. Kinet. Mech. Cat. 122 (2017) 101–115.
[59] Z. Bi, H. Zhang, X. Zhao, et al., Energy Storage Mater. 54 (2023) 313–322.